1846 *Chem. Mater.* **2010,** *22,* 1846–1853
DOI:10.1021/cm9033275

CHEMISTRY OF MATERIALS
Article

# Metal to Semimetal Transition in CaMgSi Crystals Grown from Mg−Al Flux

Jeffrey B. Whalen,[†] Julia V. Zaikina,[†] Randall Achey,[†] Ryan Stillwell,[‡] Haidong Zhou,[‡] Christopher R. Wiebe,[‡] and Susan E. Latturner*,[†]

[†]*Department of Chemistry and Biochemistry, 95 Chieftan Way, Florida State University, Tallahassee, Florida 32306, and* [‡]*National High Magnetic Field Laboratory, Florida State University, Tallahassee, Florida 32306*

*Received October 30, 2009. Revised Manuscript Received January 6, 2010*

Single crystals of CaMgSi were produced using the metal flux synthesis method in a Mg/Al 1:1 mixture. The large rod-shaped crystals measure up to 7 mm in length. This phase crystallizes with the orthorhombic TiNiSi structure type (space group *Pnma*; $a$ = 7.4752(2) Å, $b$ = 4.42720(10) Å, $c$ = 8.3149(2) Å; $R_1$ = 0.021). Despite its relationship to semiconducting Zintl phases $Mg_2Si$ and $Ca_2Si$, CaMgSi is metallic at room temperature; this produces a positive (∼160 ppm) $^{29}$Si MAS NMR chemical shift and is supported by DOS calculations. A metal to semimetal electronic transition at around 50 K is evident in the resistivity, magnetic susceptibility, and electron paramagnetic resonance measurements. Low temperature powder X-ray diffraction data indicates that a structural distortion accompanies this transition. The electronic heat capacity coefficient (0.4695 mJ/mol·K$^2$) determined from low temperature heat capacity data supports the designation of CaMgSi as a semimetal at low temperature. The hydrogen storage capacity of this phase is negligible (≤0.5 wt % hydrogen), although exposure to hydrogen does destabilize the structure, inducing decomposition at 500 °C.

## Introduction

Magnesium alloys and intermetallics are being widely investigated as potential aerospace and hydrogen storage materials because of their low expense and mass.[1] Other lightweight elements such as Si, Ca, Al, Zn, and Mn are commonly added to improve the strength and ductility of these materials.[2] This has led to growing research interest in the properties of compounds in the ternary Mg−Ca−Si system; these ternaries often occur as adventitious by-products in mixed composites. Two phases are known in this system--CaMgSi and $Ca_7Mg_{7.5\pm\delta}Si_{14}$.[3,4] A third compound, $Ca_2Mg_3Si$, was reported but later disputed; recent work in our lab has successfully produced and analyzed the hydrogen desorption of $Ca_2Mg_3Si$.[5−7] CaMgSi is commonly observed as a precipitate in Mg alloys which increases their tensile strength.[8−11] A recent report also indicates that this phase may be a promising thermoelectric material.[12] However, synthesis of single phase samples (particularly formation of single crystals) is problematic. Small crystals of CaMgSi were grown in previous studies, but measurements of physical and mechanical properties were limited by their size.[13]

In this work large single crystals of CaMgSi were reproducibly synthesized in a Mg/Al flux mixture. Metal fluxes have proven to be a useful crystal growth medium; a wide variety of intermetallics and Zintl phases can be synthesized in commonly used solvents such as Al, Ga, and Sn.[14] Our lab has been investigating mixtures of metals as fluxes. In addition to lowering the melting point of the solvent by forming eutectics, mixed fluxes introduce an

*Corresponding author. Phone: (850) 644-4074. E-mail: latturne@chem.fsu.edu.

(1) (a) Züttel, A. *Naturwissenschaften* **2004**, *91*, 157–172. (b) Sakintuna, B.; Lamari-Darkrim, F.; Hirscher, M. *Int. J. Hydrogen Energy* **2007**, *32*, 1121–1140. (c) Klyamkin, S. N. *Russ. J. Gen. Chem.* **2007**, *77*, 712–720.
(2) (a) Avedesian, M.; Baker, H. *Magnesium and Magnesium Alloys*; ASM International, Materials Park: 1998. (b) Kim, J. M.; Seong, K. D.; Jun, J. H.; Shin, K.; Kim, K. T.; Jung, W. J. *J. Alloys Compd.* **2007**, *434−435*, 324–326. (c) Park, S. S.; Bae, G. T.; Kang, D. H.; Jung, I. H.; Shin, K. S.; Kim, N. J. *Scr. Mater.* **2007**, 793–796.
(3) Axel, H.; Eisenmann, B.; Schafer, H.; Weiss, A. *Z. Naturforsch.* **1969**, *24b*, 815–817.
(4) Nesper, R.; Currao, A.; Wengert, S. *Chem.—Eur. J.* **1998**, *4*, 2251–2257.
(5) Zmiy, O. F.; Gladyshevskii, E. I. *Visn. Lviv. Derz. Univ. Se Khim.* **1969**, *11*, 38–39.
(6) Grobner, J.; Chumak, I.; Schmid-Fetzer, R. *Intermetallics* **2003**, *11*, 1065–1074.
(7) Whalen, J. B. PhD Dissertation, Florida State University, **2009**.
(8) Ben-Hamu, G.; Eliezer, D.; Shin, K. S. *Mater. Sci. Eng., A* **2007**, *447*, 35–43.
(9) Kim, J. J.; Kim, D. H.; Shin, K. S.; Kim, N. J. *Scr. Mater.* **1999**, *41*, 333–340.
(10) Ai, Y.; Luo, C. P.; Liu, J. *Acta Mater.* **2007**, *55*, 531–538.
(11) Hosono, T.; Kuramoto, M.; Matsuzawa, Y.; Momose, Y.; Maeda, Y.; Matsuyama, T.; Tatsuoka, H.; Fukuda, Y.; Hashimoto, S.; Kuwabara, H. *Appl. Surf. Sci.* **2003**, *216*, 620–624.
(12) Niwa, Y.; Todaka, Y.; Masuda, T.; Kawai, T.; Umemoto, M. *Mater. Trans.* **2009**, *50*, 1725–1729.
(13) Carbonneau, Y.; Couture, A.; Van Neste, A.; Tremblay, R. *Metall. Mater. Trans. A* **1998**, *29A*, 1759–1763.
(14) (a) Kanatzidis, M. G.; Pöttgen, R.; Jeitschko, W. *Angew. Chem., Int. Ed.* **2005**, *44*, 6996–7023.(b) Fisk, Z.; Remeika, J. P. *Handbook on the Physics and Chemistry of Rare Earths*; Gschneider Eyring, Eds.; Elsevier Science: Amsterdam, 1989; Vol. *12*, Chapter 81. (c) Fisk, Z.; Canfield, P. C. *Philos. Mag.* **1992**, *65*, 1117–1123.


Published on Web 01/29/2010

additional avenue of control over the reaction chemistry. In some cases, both components of the mixture are reactive and are incorporated into the products, as observed in the growth of $Ca_{21}Ni_2Zn_{36}$ and $Ca_6Pt_3Zn_5$ from Ca/Zn eutectic.[15] In other mixed metal solvent systems one of the flux components is inert; this is seen for several reactions in La/Ni eutectic, which yield nickel-free compounds such as $La_{21}Fe_8Sn_7C_{12}$ and $La_6Fe_9Al_4$.[16] It is also surprisingly seen in the synthesis of CaMgSi in molten Mg/Al. The Mg−Al phase diagram features a nearly uniform melting point of ~450 °C across the composition range from 62%Al:38%Mg to 30%Al:70%Mg.[17] A variety of synthetic techniques and fluxes were explored, but large single crystals of CaMgSi could only be obtained using Mg/Al as a reaction solvent. Several attempts to produce the phase from stoichiometric reactions failed and instead yielded mixed-phase polycrystalline products.

The electronic properties of CaMgSi are of particular interest. From its stoichiometry, this compound would appear to be related to the Zintl phases $Mg_2Si$ and $Ca_2Si$; it is in fact a substitutional variant of $Ca_2Si$. Magnesium silicide is a semiconductor ($E_g$ = 0.77 eV) which crystallizes in the cubic *Fm*3*m* space group.[18] The electronic properties of orthorhombic calcium silicide are less clear-cut, although most studies indicate it is also a semiconductor.[18−21] CaMgSi is therefore expected to be a Zintl phase. However, our findings indicate that this phase spans the boundary between charge balanced semiconducting Zintl phases and fully delocalized intermetallics. Exploration of materials falling between these two classifications has been of great interest in recent years, yielding compounds with unusual structures and electronic properties.[22] In the title compound, a transition from metallic to semimetal behavior is observed around 50 K, evidenced by resistivity and magnetic susceptibility measurements; this is accompanied by a structural distortion. In addition to structural and electronic characterization, hydrogenation of this phase was also investigated; little absorption was seen, but destabilization of the structure was evident.

## Experimental Section

**Synthesis.** Mg metal slugs (3.175 mm × 3.175 mm, 99.95%) and Ca shots (1 cm and down, 99.5%) were obtained from Alfa Aesar, and Si and Al powders (both 99+%) were obtained from Strem Chemicals. The elements Mg/Al/Ca/Si were weighed out in a 15/15/3/3 mmol ratio in air and placed into a niobium crucible obtained from JXMetals, Inc. (CaMgSi crystals can be synthesized in stainless steel crucibles, but this causes incorporation of Fe, Cr, and Ni impurities.) The crucible was welded shut in an argon-filled glovebox and then put into a silica tube, which was sealed under vacuum. Each reaction vessel was gently shaken several times to mix the components before being placed into the furnace. Reactions were heated from room temperature to 950 °C in 5 h, held at 950 °C for 5 h, cooled to 750 °C in 60 h, and held at 750 °C for 20 h at which point the reaction tubes were removed from the hot furnace, quickly inverted, and centrifuged. It was not necessary to use a filter in the reactions because most of the product adhered to the crucible walls. Temperature programs with different cooling times (950 to 750 °C in 30−100 h) were explored, but the optimal cooling time was found to be 60 h, which resulted in growth of the largest crystals in highest yield (90% based on Si). Cooling times longer than 100 h resulted in no crystals. Stoichiometric reactions were also explored; these produced multiphase composites of CaMgSi, $Mg_2Si$, $Ca_2Si$, and $CaMg_2$. When left out in air, the crystals show signs of surface oxidation after 1 week; they were therefore stored under argon.

**Elemental Analysis.** Samples for SEM-EDS analysis were mounted onto Al pucks with double-sided carbon tape. Elemental compositions of products were assessed using a JEOL 5900 scanning electron microscope (30 kV accelerating voltage) equipped with PGT Prism energy dispersion spectroscopy software. Analysis of the surface of the crystals did show some residual flux coating, but measurements on the interior of shattered crystals indicated a 1:1:1 molar ratio of Mg, Ca, and Si, with no aluminum or niobium present.

**X-ray Diffraction.** Single crystal X-ray diffraction data were collected on a Bruker APEX2 single crystal X-ray diffractometer with Mo Kα source. Samples were chosen by breaking the as-synthesized crystals to obtain fragments of suitable size and crystal quality. Full spheres of data were collected at 293 and 100 K under flowing nitrogen. The data were integrated by SAINT and corrected for absorption effects using the empirical method (SADABS).[23] Space group assignment was done by XPREP, and structure refinement was carried out using SHELXTL.[24] Crystallographic data and collection parameters are shown in Table 1.

Low temperature powder X-ray diffraction samples were prepared by grinding crystals in an agate mortar. Experiments were run on an original setup based on a HUBER imaging plate with Guinier camera 670 using Cu $K\alpha_1$ radiation and a Ge monochromator. Data for unit cell refinement were collected by employing a closed cycle He refrigerator system using an exposure time of 40 min at 10 to 100 K (in increments of 10 K), 150 K, 200 K, 250 K, and 270 K. The unit cell parameters were calculated from least-squares fits using the program package WinCSD.[25] A silicon internal standard was used in the collection of data sets at 298 and 10 K. Since the zero shift was the

(15) Stojanovic, M.; Latturner, S. E. *J. Solid State Chem.* **2007**, *180*, 907–914.
(16) (a) Benbow, E. M.; Dalal, N. S.; Latturner, S. E. *J. Am. Chem. Soc.* **2009**, *131*, 3349–3354. (b) Benbow, E. M.; Dalal, N. S.; Latturner, S. E. *J. Solid State Chem.* **2009**, *182*, 3055–3062.
(17) Massalski, T. B.; Okamoto, H.; Subramanian, P. R.; Kacprzak, L. *Binary Alloy Phase Diagrams*, 2nd ed.; ASM International: 1990; Vol. *1*−*3*.
(18) (a) Imai, Y.; Watanabe, A.; Mukaida, M. *J. Alloys Compd.* **2003**, *358*, 257–263. (b) Imai, Y.; Watanabe, A. *Intermetallics* **2002**, *10*, 333–341. (c) Tamura, D.; Nagai, R.; Sugimoto, K.; Udono, H.; Kikuma, I.; Tajima, H.; Ohsugi, I. J. *Thin Solid Films* **2007**, *515*, 8272–8276. (d) Morris, R. G.; Redin, R. D.; Danielson, G. C. *Phys. Rev.* **1958**, *109*, 1909–1915.
(19) Bisi, O.; Braicovich, L.; Carbone, C.; Lindau, I.; Iandelli, A.; Olcese, G. L.; Palenzona, A. *Phys. Rev. B* **1989**, *40*, 10194–10209.
(20) Ivanenko, L. I.; Shaposhnikov, V. L.; Filonov, A. B.; Krivosheeva, A. V.; Borisenko, V. E.; Migas, D. B.; Miglio, L.; Behr, G.; Schumann, J. *Thin Solid Films* **2004**, *461*, 141–147.
(21) Lebegue, S.; Arnaud, B.; Alouani, M. *Phys. Rev. B* **2005**, *72*, 085103.
(22) Corbett, J. D. *Angew. Chem., Int. Ed.* **2000**, *39*, 670.
(23) *SAINT, V. 6.02a*; Bruker AXS Inc.: Madison, WI, 2000.
(24) Sheldrick, G. M. *SHELXTL NT/2000, V. 6.1*; Bruker AXS Inc.: Madison, WI, 2000.
(25) Akselrud, L. G.; Zavalij, P. Y.; Grin, Y.; Pecharsky, V. K.; Baumgartner, B.; Wölfel, E. *Mater. Sci. Forum* **1993**, *133*−*136*, 335–351.

**Table 1. Crystallographic Data and Collection Parameters for CaMgSi at 298 K and 100 K**

| temperature | 298 K | 100 K |
|---|---|---|
| space group | *Pnma* (no. 62) | *Pnma* (no. 62) |
| cell parameter, Å | $a$ = 7.4752(2)<br>$b$ = 4.4272(1)<br>$c$ = 8.3149(2) | $a$ = 7.441(2)<br>$b$ = 4.4100(14)<br>$c$ = 8.292(3) |
| $V$, Å$^3$ | 275.175(12) | 272.09(15) |
| atom positions | Ca (0.01945(3), 1/4, 0.68077(2))<br>Si (0.27073(4), 1/4, 0.38565(3))<br>Mg (0.14423(5), 1/4, 0.06378(4)) | Ca (0.01955(4), 1/4, 0.68067(4))<br>Si (0.27059(6), 1/4, 0.38560(6))<br>Mg (0.14414(7), 1/4, 0.06382(6)) |
| $Z$ | 4 | 4 |
| density (calc), g cm$^{-3}$ | 2.232 | 2.258 |
| $\mu$, mm$^{-1}$ | 2.566 | 2.595 |
| data collection range, deg. | $3.67 < \theta < 44.84$ | $3.68 < \theta < 28.07$ |
| reflections collected | 4235 | 2789 |
| independent reflections | 1177 [$R_{int}$ = 0.0272] | 366 [$R_{int}$ = 0.0525] |
| parameters refined | 20 | 20 |
| $R_1$[a], w$R_2$[b] [$F_o > 4\sigma F_o$] | 0.0210, 0.0460 | 0.014, 0.040 |
| $R_1$, w$R_2$ (all data) | 0.0272, 0.0480 | 0.0153, 0.0402 |
| largest diff peak and hole [e/Å$^3$] | 0.429 and −0.629 | 0.305 and −0.311 |
| goodness-of-fit | 1.050 | 1.168 |

[a] $R_1 = \Sigma||F_o|-|F_c||/\Sigma|F_o|$. [b] $wR_2 = [\Sigma w(F_o^2 - F_c^2)^2/\Sigma w(F_o^2)^2]^{1/2}$, $w = [\sigma^2(F_o^2) + (A\cdot p)^2 + B\cdot p]^{-1}$; $p = (F_o^2 + 2F_c^2)/3$; $A = 0.0067$, $B = 0$.

same for a single XRD run and only the relative unit cell change with temperature was being measured, an internal standard was not used for the data collections at intermediate temperatures.

**Resistivity and Heat Capacity.** Resistivity measurements were conducted by a conventional four-point *dc* method on a Physical Property Measurement System (PPMS) by Quantum Design. Crystals (size range: 5−7 mm × 1 mm × 1 mm) were mounted on the sample holder of a $^4$He probe with a small amount of N-type Apiezon vacuum grease. Crystals were connected to the electrodes of the sample holder with 0.001 in. diameter gold wires using silver paint. Measurements were carried out from 1.8−300 K, using an applied excitation current of 1 mA. Heat capacity measurements using the PPMS were conducted on a single crystal from 4−300 K using a relaxation-time method (pulse Joule heating).

**Magnetic Susceptibility and Electron Paramagnetic Resonance.** Magnetic susceptibility data was collected on a Quantum Design SQUID Magnetic Property Measurement System. Crystals were held between two strips of kapton tape, oriented with the *c*-axis parallel to the applied field. Susceptibility data were collected at 2−300 K at an applied field of 100 G. EPR measurements were conducted on powdered samples in a conventional Bruker *X*-band (9.48 GHz) spectrometer using the appropriate resonators and modulation. The temperature was varied from 10−294 K using a helium flow cryostat temperature controller. Separate measurements were taken of the empty EPR cavity, and an empty sample holder to confirm that the signals were being produced by the sample.

**Nuclear Magnetic Resonance.** Magic angle spinning (MAS) $^{29}$Si NMR spectra were collected on a Varian Inova 500 wide-bore spectrometer. Tetramethylsilane was used as a reference. The CaMgSi crystals were ground with NaCl in a 1:1 ratio by volume to facilitate spinning of the conducting material; the mixture was packed into 4 mm zirconia rotors sealed with airtight screw caps. Data were collected at 25 °C and 4 kHz spinning rate with a single pulse sequence of 2.5 $\mu$s length and 6 s relaxation delay. The spin−lattice $T_1$ relaxation time for CaMgSi was determined using the standard inversion recovery method.

**Electronic Structure Calculations.** Calculations of band structure and density of states (DOS) were performed with the TB-LMTO-ASA program package.[26] CaMgSi crystal structure parameters determined from room temperature X-ray single crystal data were used for the calculations. Addition of empty Wigner-Seitz spheres was found to be unnecessary. The following radii of atomic spheres were used: $r$(Ca) = 2.03 Å, $r$(Mg) = 1.62 Å, and $r$(Si) = 1.55 Å. The basis set consisted of the Ca(4s, 3d), Mg(3s, 3p) and Si(3s, 3p) with Ca(4p, 4f), Mg(3d), Si(3d) being downfolded. The calculation was made for 10368 $\kappa$-points in the Brillouin zone. Integration over the Brillouin zone was made by the tetrahedron method.

**Hydrogenation and Dehydrogenation.** CaMgSi crystals were ground in an agate mortar to increase the reactive surface area of the material. Samples were then activated and hydrogenated in a lab-built volumetric pressure and temperature gas control system.[27] Activation of the powder was carried out by heating under dynamic vacuum for 30 min at 450 °C. Hydrogen gas was then introduced into the sample chamber at 37.4 atm (550 psig) and 450 °C. The sample chamber pressure was automatically readjusted by the apparatus every 30 s for 15 intervals. When complete, the samples were removed from the sample chamber and analyzed using TGA/DSC analysis with a TA Instruments SDT 2960 Simultaneous DSC-TGA. The samples were heated to 520 at 5 °C/min and then held at 520 °C for 30 min. Identical DSC/TGA measurements were carried out on $MgH_2$ from Alfa Aesar as a standard hydride comparison.

## Results and Discussion

Magnesium-based fluxes have not been widely investigated as synthesis media because of their volatility and corrosive nature. Our use of sealed steel or niobium ampules allows for containment of the Mg vapors and facilitates flux growth of Mg-containing products. The Mg/Al flux mixture solidifies at 450 °C, but it is very viscous and difficult to remove well above this temperature. Therefore the ampules were removed from the furnace at 750 °C to ensure that the flux remained in its molten state during transfer of the reaction vessel from the furnace to the centrifuge. After centrifugation and cooling of the reaction vessels, the excess flux is found solidified in the end of the crucible which indicates successful separation. The crystals are found adhered to the wall of the crucibles on the opposite end. The maximum size of the crystals appears to be limited only by the diameter of the crucible.

The use of a stoichiometric reaction does not result in formation of the pure CaMgSi phase, instead yielding mixed-phase powders of CaMgSi, $Mg_2Si$, $Ca_2Si$, and $CaMg_2$. Reactions in pure magnesium flux also do not yield the title compound. Aluminum may promote the reaction by acting as either a transport agent within the flux, a destabilizing agent (which hinders the formation of $Mg_2Ca$ and $Mg_2Si$ by retaining Mg in the excess flux solution), or a solvent for the incorporation of elements with low solubility in molten Mg. Aluminum metal has

(26) Jepsen, O.; Burkhardt, A.; Andersen, O. K. *The Program TB-LMTO-ASA, version 4.7*; Max-Planck-Institut für Festkörperforschung: Stuttgart, Germany, 2000.
(27) Whalen, J.; Greska, B.; Latturner, S. E. Manuscript in preparation.

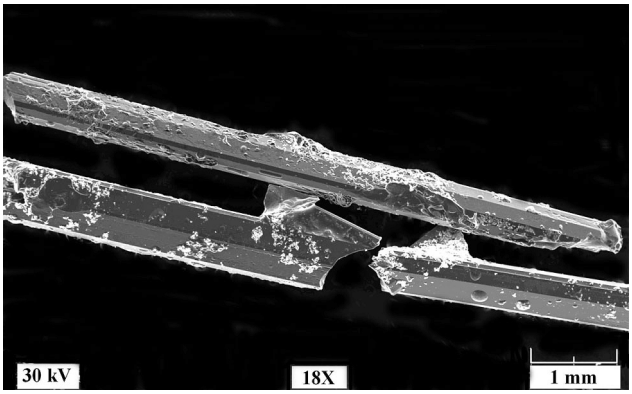


**Figure 1.** SEM image of representative crystals of CaMgSi grown in Mg/Al flux.

been shown in the literature to be a highly reactive solvent, facilitating the growth of aluminide intermetallics.[14,28] However, in this case, Al incorporation was not detected by EDS analysis of the CaMgSi product, which indicates that its concentration in the crystals was extremely low. It is possible that ppm/ppb amounts of Al were incorporated into the structure via substitution on the Mg or Si site. In the crystallographic data refinement, the occupancy of these sites was allowed to vary but did not deviate significantly from unity. Detection of Al by glow-discharge or inductively coupled plasma mass spectrometry would not distinguish actual Al doping in the structure from residual Mg/Al flux on the surface of crystals, so this analysis was not employed. The existence of many Mg−Al binary phases, and no known Al−Si phases, might rationalize why the Al metal is retained in the flux. Other magnesium-based flux mixtures Mg/X (X = Li, Ca, Ni, Cu, Zn, Ga, Sn, Sb, In, Pb, Bi) were also explored as solvents in reactions targeting CaMgSi; however, the phase was only produced in the Mg/Al flux.

Figure 1 shows an SEM image of several large CaMgSi crystals (approximately 7 mm × 1 mm × 1 mm) which are actually broken fragments of larger crystals. Small amounts of Mg−Al flux are adhered to regions on the surface of the crystals; these areas were not targeted during elemental analysis. Analyses on several cleaved surfaces show an average mole percent composition of 33(2)% Mg, 36(2)% Si, and 31(2)% Ca. An earlier study indicated a small phase width to the calcium-rich side is possible for this compound ($Mg_{1-x}Ca_{1+x}Si$, $x \leq 0.07$),[6] but unit cell parameters of CaMgSi crystals from many different Mg/Al flux reactions had nearly identical values within estimated standard deviation. Given the Mg-rich synthesis medium used in our work, only the Mg-rich composition was obtained and phase width was not observed.

**Structural Features.** CaMgSi crystallizes in the orthorhombic TiNiSi structure type, a ternary variant of the $Co_2Si$ or anti-$PbCl_2$ structure type. Atom positions and unit cell parameters are listed in Table 1, and the structure

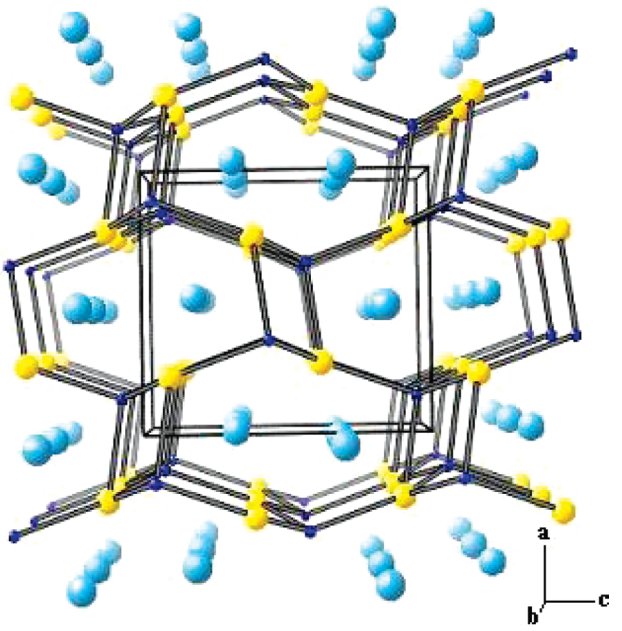


**Figure 2.** CaMgSi crystal structure viewed down the *b*-axis. Large light blue spheres are Ca atoms, yellow spheres are Mg, and small blue spheres are Si.

is shown in Figure 2. The structure is formed from the complete substitution of Mg for Ca on one of the 4*c* sites in the $Ca_2Si$ ($Co_2Si$ type) structure. This results in the formation of a three-dimensional Mg/Si network forming channels in which the calcium cations reside. Both the Mg and Si sites are four-bonded, with highly distorted tetrahedral coordination. The TiNiSi structure type is common for ternary intermetallic phases RTX with a 1:1:1 ratio of an electropositive metal (R = rare earth, alkaline earth, early transition metal), a late transition metal T, and a main group element X (X = Si, Ga, Al, Sn, etc.). In the hundreds of phases comprising this family of compounds, the electropositive R metal cation occupies the channels formed from the T/X framework.[29]

This structure is clearly stable for a wide range of valence electron counts, and deriving a Zintl phase model of electron transfer from the R metal to the T/X framework is not applicable in most cases.[30] In spite of this, it is tempting to view CaMgSi as a Zintl phase. It is derived from $Ca_2Si$, which from its stoichiometry, atomic coordination, and semiconducting properties can be viewed as $(Ca^{2+})_2(Si^{4-})$. Replacing one calcium ion with a $Mg^{2+}$ ion should lead to another semiconducting Zintl phase. However, magnesium often does not behave like an alkaline earth metal in alloys and intermetallics. Incorporation of magnesium into TiNiSi structure phases has been recently observed in compounds such as EuMgT (T = Ag, Au, Tl, Pd, Si, Ge, Sn, Pb), CaMgPd, and YbMgAg, with Mg occupying a site in the "anionic" T/X network.[31,32] While

(28) (a) Latturner, S. E.; Kanatzidis, M. G. *Inorg. Chem.* **2008**, *47*, 2089–2097. (b) Latturner, S. E.; Bilc, D.; Mahanti, S. D.; Kanatzidis, M. G. *Inorg. Chem.* **2009**, *48*, 1346–1355. (c) Kauzlarich, S. M.; Condron, C. L.; Wassei, J. K.; Ikeda, T.; Snyder, G. J. *J. Solid State Chem.* **2009**, *182*, 240–245.

(29) Landrum, G. A.; Hoffmann, R.; Evers, J.; Boysen, H. *Inorg. Chem.* **1998**, *37*, 5754–5763.

(30) Kauzlarich, S. *Structure and Bonding of Zintl Phases and Ions*; VCH Publishers: New York, 1996.

(31) Rodewald, U. C.; Chevalier, B.; Pöttgen, R. *J. Solid State Chem.* **2007**, *180*, 1720–1736.

(32) Fornasini, M. L.; Merlo, F.; Napoletano, M.; Pani, M. *J. Phase Equilib.* **2002**, *23*, 57–60.

these RMgX phases do appear to favor formation with a divalent R element, they vary in their overall valence electron count and are metallic. CaMgSi also has Mg bonded to Si to form the "anionic" network with short Mg−Si bonds of 2.7382(3) − 2.8234(5) Å. This would indicate this phase is in the same polar intermetallic class as the other RMgX phases. The electronic properties of CaMgSi were studied to determine if this compound behaves as a semiconducting Zintl phase or an intermetallic.

**Solid State MAS NMR.** Solid state $^{29}$Si MAS NMR was used to characterize the electronic environment of silicon in the compound. One broad peak was observed (see Supporting Information Figure S1), in agreement with the single Si crystallographic site in the structure. The positive chemical shift of 160 ppm is far from the −177 ppm resonance observed for semiconducting $Mg_2Si$.[33] Other silicide Zintl phases are also characterized by negative $^{29}$Si NMR shifts; the $M_4Si_4$ family (M = Na, K, Rb, Cs) has resonances in the −280 to −360 ppm region.[34,35] Semiconducting low-sodium silicon clathrates $Na_xSi_{136}$ and doped silicon have resonances falling in the values of −100 to +100 ppm; this range can be classified as the chemical shift region for covalently bonded semiconducting silicon.[36] The silicon framework atoms of metallic clathrates such as $Na_8Si_{46}$ and $Na_{16}Rb_8Si_{136}$ exhibit Knight shifts due to the conduction electrons in these phases; all their $^{29}$Si resonances occur from 200 ppm up to 1000 ppm.[37] Other metallic silicides also have $^{29}$Si Knight shifts in this region, such as $Ba_3Si_4$ (281 ppm) and $Y_5Si_2B_8$ (217 ppm).[38,39] The 160 ppm peak observed for CaMgSi is on the border of the Knight shift region and far from the diamagnetic shifts seen for Zintl phases. This indicates metallic behavior. Additional evidence comes from the observed $T_1$ spin−lattice relaxation time of 4 s for the $^{29}$Si nuclei in CaMgSi. This rapid relaxation is facilitated by the conduction electrons and is orders of magnitude shorter than the long $^{29}$Si relaxation times characteristic of diamagnetic semiconducting silicide phases such as $Mg_2Si$ ($T_1$ = 600 s).[33,34]

**Electronic Structure Calculations.** The calculated density of states (DOS) for CaMgSi is shown in Figure 3; the associated band structure diagram can be found in the Supporting Information. The analysis of total DOS reveals that while there is a pronounced pseudogap at the Fermi level ($E_F$), the compound is still intrinsically

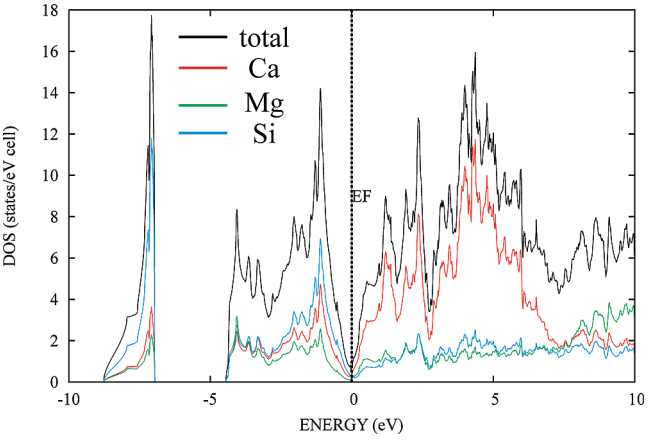


**Figure 3.** Total and partial density of states for CaMgSi. Contributions from different atoms are color-coded.

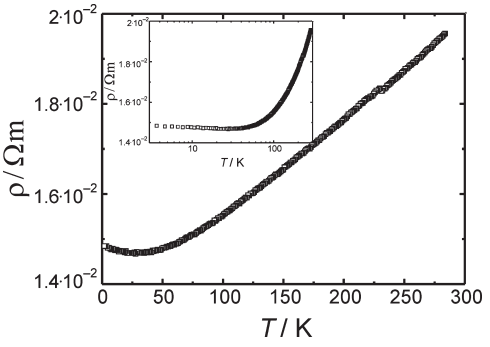


**Figure 4.** Temperature dependence of resistivity; inset shows resistivity vs log temperature ($\rho$ vs log $T$).

metallic. Ca, Mg, and Si contribute to the states near $E_F$ nearly equally. This indicates significant cation−anion orbital mixing (hybridization), which leads to the closing of the gap at the Fermi level and metallic behavior, in agreement with the room temperature $^{29}$Si NMR data. Resistivity measurements were carried out to explore the temperature dependence of the electronic properties.

**Resistivity Measurements.** Resistivity data from 0.65 to 300 K are shown in Figure 4 with temperature axis in both regular and log scale form. At high temperatures, the resistivity of CaMgSi has a metallic-like dependence on temperature. The change in slope of the plot at 50 K indicates that a variation in the electronic behavior occurs in this temperature range. Compounds with metal-to-semiconductor electronic transitions, such as $Sc_3B_{0.75}C_3$ and $Ba_3Si_4$, also display minima in their resistivity plots at temperatures of 50 K and 30 K, respectively.[38,40] The room temperature resistivity of CaMgSi is 1.95 Ω·cm; this value lies in the overlap of typical metallic ($10^{-5}$–$10^{1}$ Ω·cm) and semiconductor ($10^{-2}$–$10^{5}$ Ω·cm) resistivity ranges.[41] $Sc_3B_{0.75}C_3$ and $Ba_3Si_4$ have similar resistivities above their transition temperatures (room temperature resistivities of 0.185 and 1.20 Ω·cm, respectively). Magnetic susceptibility, low temperature diffraction, and heat

(33) Ratai, E.; Augustine, M. P.; Kauzlarich, S. M. *J. Phys. Chem. B* **2003**, *107*, 12573–12577.
(34) Mayeri, D.; Phillips, B. L.; Augustine, M. P.; Kauzlarich, S. M. *Chem. Mater.* **2001**, *13*, 765–770.
(35) Stearns, L. A.; Gryko, J.; Diefenbacher, J.; Ramachandran, G. K.; McMillan, P. F. *J. Solid State Chem.* **2003**, *173*, 251–258.
(36) Pouchard, M.; Cros, C.; Hagenmuller, P.; Reny, E.; Ammar, A.; Menetrier, M.; Bassat, J. M. *Solid State Sci.* **2002**, *4*, 723–729.
(37) Latturner, S. E.; Iversen, B. B.; Sepa, J.; Srdanov, V.; Stucky, G. *Phys. Rev. B* **2001**, *63*, 125403.
(38) Aydemir, U.; Ormeci, A.; Borrmann, H.; Bohme, B.; Zurcher, F.; Uslu, B.; Goebel, T.; Schnelle, W.; Simon, P.; Carrillo-Cabrera, W.; Haarmann, F.; Baitinger, M.; Nesper, R.; Von Schnering, G. H.; Grin, Y. *Z. Anorg. Allg. Chem.* **2008**, *634*, 1651–1661.
(39) Roger, J.; Babizhetsky, V.; Cordier, S.; Bauer, J.; Hiebl, K.; Le Polles, L.; Ashbrook, S. E.; Halet, J. F.; Guerin, R. *J. Solid State Chem.* **2005**, *178*, 1851–1863.
(40) Mori, T.; Shi, Y.; Tanaka, T. *J. Alloys Compd.* **2000**, *308*, 115–120.
(41) West, A. R. *Basic Solid State Chemistry*, 2nd ed.; John Wiley & Sons, Ltd.: Chichester, West Sussex, England, 1999.

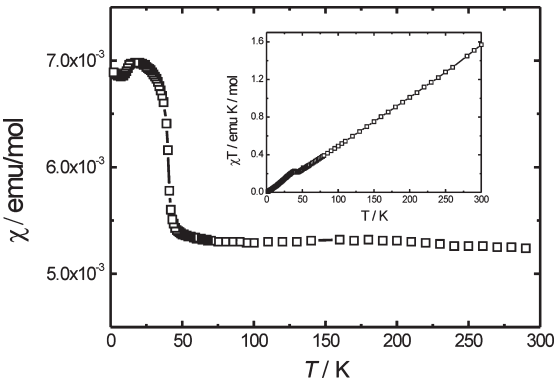


**Figure 5.** Temperature dependence of magnetic susceptibility of CaMgSi (inset shows $\chi T$ vs $T$).

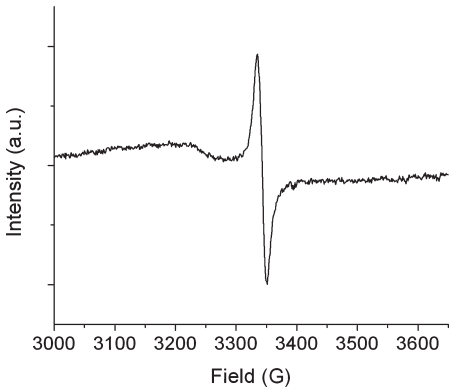


**Figure 6.** X-band EPR spectrum of CaMgSi taken at 20 K showing the sharp resonance from localized electrons and a broad signal from conduction electrons.

capacity studies were carried out to further characterize the temperature dependence of the electronic behavior and the nature of the compound below the observed transition.

**Magnetic Susceptibility and Electron Paramagnetic Resonance.** The high temperature molar susceptibility of CaMgSi is small, positive, and independent of temperature, as shown in Figure 5. This is consistent with Pauli paramagnetism due to delocalized conduction electrons. A plot of $\chi T$ vs $T$ yields a line which intersects both axes at 0 K (Figure 5, inset), also indicative of Pauli paramagnetism. As the material is cooled below 50 K there is a sharp increase in the magnetic susceptibility; this occurs at the temperature range corresponding to the local minimum in the resistivity data (Figure 4b). This sharp increase in susceptibility is attributed to localization of conduction electrons on defect sites in the structure. Similar behavior is seen in another compound, $Sc_3B_{0.75}C_3$; a jump in the susceptibility is seen at the same temperature as a metal-to-insulator transition which the authors postulate may be due to a change in structure.[40] A localization phenomenon has also been theorized to explain similar variations in resistivity and susceptibility for $Ca_7Mg_{7.5\pm\delta}Si_{14}$.[4]

EPR measurements were carried out to confirm the localization of electrons below the transition. The low temperature EPR spectra indicate the presence of both localized electrons (yielding a narrow peak with an integral peakwidth of 70 G fwhm) and delocalized electrons (producing a very broad low intensity signal); a representative spectrum taken at 20 K (see Figure 6) shows both resonances. Both have temperature independent $g$-values. The intensity of the narrow peak (not observed in high temperature spectra; see Supporting Information Figure S2) rises dramatically below 50 K. The EPR and susceptibility data indicate that the compound is a metal at high temperatures. Below 50 K, a transition occurs which does not eliminate the conduction electrons; the compound is therefore in a semimetal state but is not a semiconductor. The appearance of the sharp resonance indicates the localization of some electrons, possibly on defect states in the pseudogap which may be due to aluminum incorporation. Substitution of Al onto silicon sites would produce hole trap sites in the structure which would not be associated with the normal band structure of the compound. Electrons present in these trap sites would behave as paramagnetic localized electrons, giving rise to the sharp EPR resonance and the increased susceptibility below 50 K.

**Structural Distortion at Low Temperature.** Powder X-ray diffraction data were collected from room temperature down to 10 K to determine if the electronic transition is accompanied by a structure change. All peaks could be indexed in the primitive orthorhombic unit cell of the TiNiSi structure; no evidence of a change of symmetry (such as peak splitting or appearance of new peaks) was observed at any temperature. As the sample is cooled to 10 K, the unit cell parameters decrease due to the expected thermal contraction of the cell volume (Figure 7). The overall decreases in unit cell parameters were most significant for the $a$-axis: $\Delta a = 0.0212$ Å, $\Delta b = 0.0118$ Å, $\Delta c = 0.0151$ Å, and $\Delta V = 1.943$ Å$^3$. The structure can be viewed as puckered hexagonal Mg−Si sheets stacked along the $a$-axis and pinned together. The shrinking of the $a$-axis reduces the interlayer spacing with decreasing temperature. However, these decreasing parameters show a distinct change in slope at 50 K. The temperature dependencies of resistivity and unit cell parameters result in very similar shaped plots, having slope changing features at the same temperature range. Therefore, this deviation from linear thermal contraction is correlated to the change in electronic structure. To examine the nature of the structural distortion, Rietveld analysis was attempted to pinpoint the changes in atomic coordinates, but the quality of the data was limited by the diffractometer and results were unreliable. Heat capacity measurements were carried out to further characterize the behavior of the material at the temperature of this transition and below.

**Heat Capacity.** The heat capacity data for CaMgSi are shown in the Supporting Information (Figure S3). Heat capacity can be separated into two components, an electronic contribution and a lattice vibration contribution; this is indicated by the equation $C_p = \gamma T + \beta T^3$. The coefficients $\gamma$ and $\beta$ quantify the contributions of electrons at $E_F$ and phonons, respectively; these can be derived from a linear fit of $C_p/T$ vs $T^2$ at low temperatures. Below 9 K, the $C_p/T$ vs $T^2$ plot for CaMgSi is linear, and the resulting electronic ($\gamma$) and lattice ($\beta$) heat capacity coefficients are $\gamma = 0.4695$ mJ/mol·K$^2$ and $\beta = 0.04033$ mJ/mol·K$^4$.

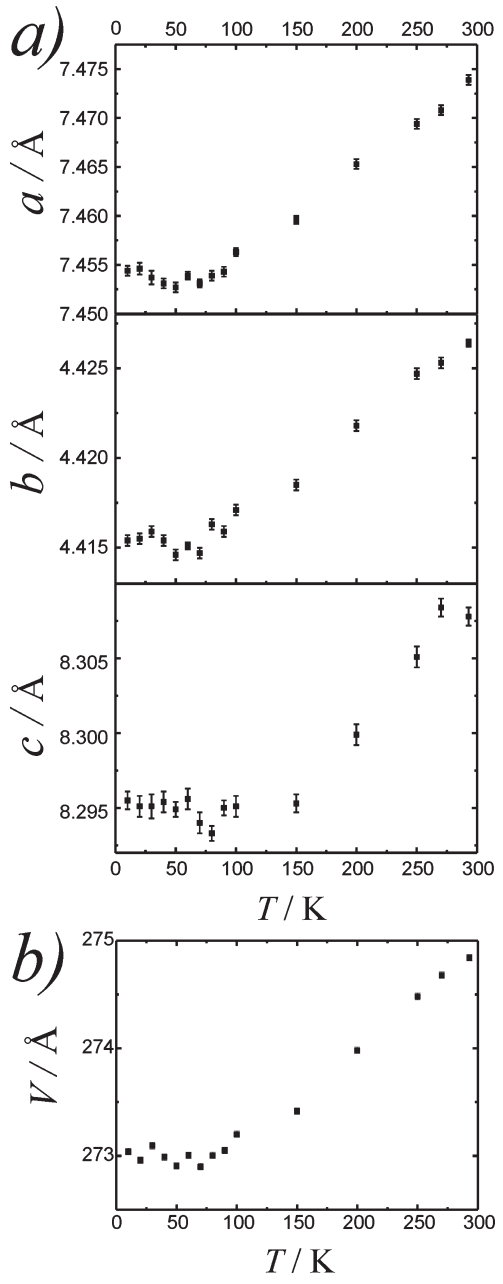


**Figure 7.** Temperature dependence of *a*, *b*, and *c* unit cell parameters and unit cell volume (*V*) for CaMgSi.

The observed $\gamma$ values for metallic elements and compounds are usually above 0.6 mJ/mol·K$^2$; elemental Mg and Ca have $\gamma$ = 1.3 and 2.9 mJ/mol·K$^2$, respectively.[42,43] Semimetals are often characterized by $\gamma$ values in the 0 to 0.2 mJ/mol·K$^2$ range; for instance, elemental Bi has a $\gamma$ value of 0.008 mJ/mol·K$^2$.[43] At low temperatures, CaMgSi has an intermediate value, indicating it is definitely not a semiconductor (the $\gamma$ value for semiconducting $Mg_2Si$ is considered negligible[44]), and can more appropriately be classified as a semimetal. Therefore, the observed changes in resistivity and magnetic susceptibility are likely to be the result of a metal to semimetal transition. From the value of $\gamma$, the total density of states at the Fermi level ($N(E_F)$) was calculated as 0.80 states/eV·unit cell. This is in good agreement with the $N(E_F)$ derived from density of states calculations (see Figure 3); both indicate a pseudogap at $E_F$. The $\beta$ value was used to calculate a Debye temperature ($\theta_D$) of 525 K for CaMgSi. Elemental Mg, Ca, and Si have $\theta_D$ values of 318 K, 230 K, and 625 K, respectively.[43] The value for CaMgSi indicates a stiffer lattice than that of pure Mg or Ca. $Mg_2Si$, with a $\theta_D$ of 578 K, has a stiffer lattice than CaMgSi.[44]

The transition of CaMgSi from metal to semimetal does not result in a sharp change in heat capacity; no anomalies in the heat capacity data were observed near 50 K. This indicates that this structural distortion and the accompanying electronic modification is not a first order phase transition but is instead more subtle. One phenomenon that could possibly explain these observations is the formation of a charge density wave (CDW) in the compound at low temperature. A CDW is a modulation of electronic charge in the Fermi sea of metals, accompanied by an aperiodic pattern of atomic displacements; this produces an energy gap at the Fermi surface. The formation of a CDW gap below 50 K in CaMgSi may facilitate uncovering of the defect states near the pseudogap, allowing localization of some of the conduction electrons. Development of a CDW would be averaged out in the powder diffraction data and may not be observed in the heat capacity data. Previous studies of the known CDW in $\gamma$-$Mo_4O_{11}$ also do not show any abnormal features in the heat capacity plots.[45−47] Single crystal XRD below the transition temperature would be necessary to investigate this.

**Hydrogen Absorption and Thermal Stability.** CaMgSi has previously been reported to have very little hydrogen absorption capability.[48] Poor hydrogen absorption could be a result of the contracted structure of the phase which has minimal interstitial space to accommodate hydrogen atoms. After exposure to 37.4 atm $H_2$ at 450 °C, the thermogravimetric data for CaMgSi shows very little weight loss from room temperature through 500 °C (less than 0.5% for multiple sample runs). Decomposition of the compound occurred above 500 °C; powder XRD data for these dehydrogenated samples indicates formation of elemental Mg and $Ca_2Si$. Magnesium dendrites are also visually apparent on the surface of the samples after this process. CaMgSi crystals which had not been hydrogenated do not exhibit the same behavior upon heating, remaining stable up to 1000 °C (the maximum temperature applied in the TGA). This is consistent with previous reports stating that CaMgSi melts congruently at 1234 °C.[6] Absorption of even a trace of hydrogen evidently destabilizes the structure of this compound; release of hydrogen

(42) Kittel, C. *Introduction to Solid State Physics*, 6th ed.; John Wiley & Sons, Inc.: New York, 1986.
(43) Ashcroft, N. W.; Mermin, N. D. *Solid State Physics*; Cornell University, Brooks/Cole Thomson Learning: United States, 1976.
(44) Gerstein, B. C.; Jelinek, F. J.; Habenschuss, M.; Shickell, W. D.; Mullaly, J. R.; Chung, P. L. *J. Chem. Phys.* **1967**, *47*, 2109–2115.
(45) Da Luz, M. S.; De Campos, A.; White, B. D.; Neumeier, J. J. *Phys. Rev. B* **2009**, *79*, 233106.
(46) Greenblatt, M. *Chem. Rev.* **1988**, *88*, 31–53.
(47) Guyot, H.; Schlenker, C.; Fourcaudot, G.; Konate, K. *Solid State Commun.* **1985**, *54*, 909.
(48) Wu, H.; Zhou, W.; Udovic, T. J.; Rush, J. J. *J. Alloys Compd.* **2007**, *446−447*, 101–105.

from $CaMgSiH_x$ induces an irreversible disproportionation reaction which causes the release of Mg and formation of the more stable binary compound, $Ca_2Si$. Similar destabilization and formation of $MgH_2$ whiskers (which convert to Mg dendrites upon dehydrogenation) has been observed for $Mg_{24}Y_5$.[49,50]

## Conclusions

Mg/Al mixed flux provides a unique crystal growth environment which allows the formation of large crystals of CaMgSi which cannot be synthesized using other methods. The size of these crystals enables the use of a variety of characterization techniques which have shown that this phase behaves like an intermetallic at high temperatures but undergoes a metal to semimetal transition at 50 K which is associated with the localization of some of the conduction electrons at defect sites in the structure. This is accompanied by a subtle structural distortion which may occur as a charge density wave. Synthesis of these phases without aluminum is needed to determine if the distortion and electronic modifications occur in the absence of low levels of dopant. Several RMgT analogs (R = Ca, Sr; T = Si, Ge, Sn) can be grown from Mg/Al eutectic and may also be susceptible to these distortions and their accompanying electronic modifications.

**Acknowledgment.** The authors thank Dr. K. Kovnir for assistance with band structure calculations. We thank Dr. Jurek Krzystek of the NHMFL for assistance with the EPR data collection. We thank Prof. Gordon Miller (Iowa State University) for useful discussions. This research was supported by the National Science Foundation (grant award number DMR-05-47791). C.R.W. acknowledges support from the NSF (DMR-0084173). Use of the Tozer group Open Door Laboratory facilities at NHMFL was made possible by support from DOE/NNSA (grant number DE-FG52-06NA26193, NSF, and the State of Florida).

**Supporting Information Available:** Crystallographic data for CaMgSi, in the form of CIF files, room temperature $^{29}Si$ MAS NMR spectrum, variable temperature EPR data, heat capacity data, and band structure diagram for CaMgSi at room temperature. This material is available free of charge via the Internet at http://pubs.acs.org.

(49) Zlotea, C.; Lu, J.; Andersson, Y. *J. Alloys Compd.* **2006**, *426*, 357–362.
(50) Zlotea, C.; Sahlberg, M.; Oezbilen, S.; Moretto, P.; Andersson, Y. *Acta Mater.* **2008**, *56*, 2421–2428.